Chapter 4 Propagation of plasma L-phenylalanine concentration fluctuations to the neurovascular unit in phenylketonuria: An *in silico* study.

This chapter has been submitted for publication:

Mehdi Taslimifar, Stefano Buoso, François Verrey, and Vartan Kurtcuoglu "Propagation of plasma L-phenylalanine concentration fluctuations to the neurovascular unit in phenylketonuria: An *in silico* study".

Abstract

Phenylketonuria (PKU) is an inherited metabolic disease characterized by abnormally high concentrations of the essential amino acid L-phenylalanine (Phe) in blood plasma caused by reduced activity of phenylalanine hydroxylase (PAH). While numerous studies have shown association between high plasma Phe concentration and intellectual impairment, it is not clear whether increased Phe fluctuations also observed in PKU affect the brain as well. To investigate this, time-resolved in vivo data on Phe and competing large neutral amino acid (LNAA) concentrations in neurons are needed, but cannot be acquired readily with current methods. We have used in silico modeling as an alternative approach to characterize the interactive dynamics of Phe and competing LNAAs (CL) in the neurovascular unit (NVU). Our results suggest that plasma Phe fluctuations can propagate into the NVU cells and change there the concentration of LNAAs, with the highest magnitude of this effect observed at low frequency and high amplitude-to-mean ratio of the plasma Phe concentration fluctuations. Our model further elucidates the effect of therapeutic LNAA supplementation in PKU, showing how abnormal concentrations of Phe and CL in the NVU move thereby towards normal physiologic levels.

Keywords: Phenylketonuria, L-phenylalanine fluctuation, neurovascular unit, amino acid transporter, large neutral amino acid

Introduction

Phenylketonuria (PKU) is the most common disorder of amino acid (AA) metabolism, resulting from a severely reduced activity of the liver enzyme phenylalanine hydroxylase (PAH), which leads to abnormal accumulation of the essential amino acid L-phenylalanine (Phe) in the blood plasma [37, 129]. Phe is transported across the blood brain barrier (BBB) into the neurovascular unit (NVU), where abnormal increase in its concentration leads to imbalance of large neutral amino acid (LNAA) levels in brain interstitial fluid (ISF), astrocytes and neurons, as a consequence of the competition for NVU-LNAA transporters [130]. Since NVU-LNAAs are required for the synthesis of essential neurotransmitters such as dopamine, serotonin, and norepinephrine, their perturbations can lead to intellectual disabilities, growth abnormalities and severe behavioral problems in PKU patients [129].

The dysfunction of the PAH enzyme is also the cause of higher than normal fluctuations in Phe plasma concentration, where patterns greatly vary among patients in relation to age, diet, genotype and level of PAH defect [38, 131]. Nevertheless, only time-averaged Phe concentrations are used to classify PKU severity (benign, mild or classic) and design the treatment protocol, which consists mainly of a low Phe diet to reduce mean blood Phe concentration [38, 132]. However, the effectiveness of such therapies depends on the concentrations of LNAAs in the NVU, which can influence brain function and behavior, rather than directly the blood Phe level [38]. Some studies have specifically investigated the relation between brain function (assessed through intelligence quotient (IQ) tests) and mean plasma Phe concentration and its fluctuations. The results were not conclusive: while in some studies IQ was found to be more often associated with the level of Phe fluctuations in the plasma rather than with its mean value [133, 134], the opposite was reported in others [135, 136], while no differentiation was possible in yet another one [131]. The reasons for this inconsistency are not clear, but could be, in part, a reflection of how fluctuations in plasma Phe concentration translate in individual patients to effects on AA homeostasis in the brain [38].

The propagation of Phe fluctuations from plasma into the brain is critically influenced by the competition between this AA and its competing LNAAs (CL, i.e. L-leucine, L-isoleucine, L-tyrosine, L-tryptophan, L-valine, L-histidine and L-methionine) for transporters at NVU cell membranes [137]. It has been shown that the Na^+-

independent antiporter SLC7A5 (LAT1) in microvascular brain endothelial cells (MBEC) [24-26], the Na^+-independent antiporter SLC7A8 (LAT2) in astrocytes [27-29], and the Na^+-dependent symporter SLC6A15 (B^0AT2) in neurons [30-32] are the main regulators of LNAAs homeostasis in the NVU (Figure 1). *In vivo* monitoring of LNAA levels in individual NVU compartments during fluctuations of plasma Phe concentrations could help establish a better understanding of their interrelation, but there are technological hurdles that need to be overcome to enable corresponding experiments.

To go around these hurdles, we have employed a previously developed computational model of NVU-LNAAs homeostasis [137] to explore *in silico* how plasma Phe fluctuations influence LNAA concentrations in the NVU. In addition, we have quantified the variations in concentration of Phe and CL in NVU cells in relation to descriptors of plasma Phe fluctuation, namely mean, fundamental frequency and amplitude-to-mean ratio [38, 138]. Finally, we have employed the model to explore the impact of therapeutic supplementation of LNAAs on the attenuation of Phe and CL concentrations in NVU cells. While this treatment strategy has been shown to modulate the perturbed concentration of LNAAs in brain tissue in a PKU mouse model [139, 140] and also to positively impact executive functioning of PKU patients [141, 142], it remains unclear how supplementation of LNAAs affects the dynamics of Phe and CL concentration in MBECs, astrocyte and more importantly in neurons [139, 142].

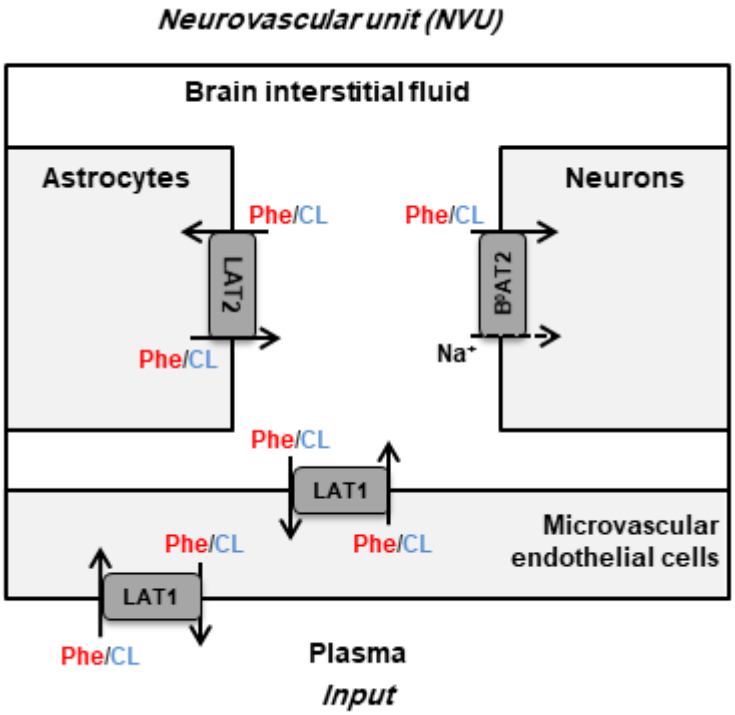

Figure 4.1. Schematic representation of the neurovascular unit and the therein expressed dominant Phe and CL transporters. The dominant Phe and CL transporters involved in the pathophysiology of PKU disorder include the Na^+-independent antiporter LAT1 (SLC7A5) in MBECs, the Na^+-independent antiporter LAT2 (SLC7A8) in astrocytes and the Na^+-dependent symporter B^0AT2 (SLC6A15) in neurons. The arrows specify Phe and CL transmembrane pathways. The plasma concentration profiles of Phe and CL are taken as the input to the neurovascular unit (NVU), based on which concentrations in the NVU compartments are calculated.

Methods

We employed a previously developed compartmental model of NVU-LNAA homeostasis in adult rats [137], to which we refer the reader for detail. Four NVU individual compartments are considered – MBECs, ISF, astrocytes (ast), and neurons (neu) – within which LNAAs are assumed to be homogeneously distributed (Fig. 4.1). In the model, LNAA fluxes between compartments are mediated by the dominant transporters identified from literature, i.e. LAT1, LAT2 and B^0AT2 (Table 4.1). Fluxes mediated by the antiporters LAT1 and LAT2 are a function of the following: maximum transport rates at the BBB luminal (lum) ($V_{max,LAT1,lum}$) and abluminal (abl) ($V_{max,LAT1,abl}$) membranes and astrocyte membrane ($V_{max,LAT2}$), respectively; Michaelis-Menten binding constants in the individual NVU compartments

($K_{m,LAT1}{}^{P(MBEC,ISF)}$ and $K_{m,LAT2}{}^{ISF(Ast)}$); and the LAT1 bi-directional kinetic constant (RK_{LAT1}), which corresponds to the ratio between the absolute Michaelis-Menten binding constant for LAT1 in MBECs relative to the corresponding value in the ISF and in plasma ($\frac{K_{m,abs,LAT1}{}^{MBEC}}{K_{m,abs,LAT1}{}^{P(ISF)}}$) [137]. The fluxes mediated by B^0AT2 symporter are a function of Michaelis-Menten kinetic parameters (V_{max,B^0AT2} and $K_{m,B^0AT2}{}^{ISF(Neu)}$); neuronal electrical potential-induced biases for forward and backward transport rates (ε and ε'); neuronal potential difference ($\Delta\psi$), electrical bias constant (β), Faraday constant (F), sodium charge (z), gas constant (R) and absolute temperature (T) (see [137] for details). To account for the approximate 1:1 stoichiometry observed for LAT1 and LAT2 antiporters under normal physiologic conditions [26, 33], at each instant we limited Phe and CL fluxes to the lowest value between the two. The values of kinetic parameters and compartment volumes (V_i) used in the model are taken from literature, and are reported in Table 4.1. The same values are considered for both PKU and normal physiologic cases [137, 143].

Model calculations were performed as follows: We first determined steady state (ss) concentrations of Phe and CL in the individual NVU compartments *i* ($[Phe]_{ss}^{i}$ and $[CL]_{ss}^{i}$) by prescribing constant plasma concentrations ($[Phe]_{ss}^{P}$ and $[CL]_{ss}^{P}$) as model inputs and initializing the concentrations in the NVU compartments based on steady state concentration values reported in [137]. We considered plasma Phe concentrations from 77 μM (representing normal physiologic condition) [84] to values above 1200 μM (representing sever classic PKU) [129]. Plasma CL concentration was kept constant at 739 μM [84, 92].

We then prescribed fluctuating plasma Phe concentrations as

$$[Phe]_f^P = [Phe]_{ss}^P\left(1 + c_f \frac{[Phe]_\delta^P}{max|[Phe]_\delta^P|}\right), \quad 1$$

where c_f is a coefficient that can take on values between 0 and 1, and thereby scales the fluctuation amplitude (relative to mean), and $[Phe]_\delta^P$ is a periodic zero-mean fluctuating component with zero initial value described by the trigonometric Fourier series

$$[\mathrm{Phe}]_{\delta}^{\mathrm{P}} = \sum_{n=1}^{N} a_n \sin(2\pi n f_0 t) + b_n \cos(2\pi n f_0 t), \quad (2)$$

where n is an integer, f_0 is the fundamental frequency of Phe fluctuation, and a_n and b_n are the Fourier coefficients.

For presentation purposes, we initially considered three distinct plasma Phe fluctuation profiles referred to as cases c1 to c3, with values of steady state concentration, frequency and relative amplitude as given in Table 4.2. For each of these cases, we determined the steady state concentrations of Phe and CL ($[\mathrm{Phe}]_{\mathrm{ss}}^{\mathrm{i}}$ and $[\mathrm{CL}]_{\mathrm{ss}}^{\mathrm{i}}$) as well as the fluctuating response ($[\mathrm{Phe}]_{\mathrm{f}}^{\mathrm{i}}$ and $[\mathrm{CL}]_{\mathrm{f}}^{\mathrm{i}}$) in the NVU compartments. Results for this *in silico* investigation are shown as time series (excluding the initial transition from the steady state) normalized with respect to the corresponding values for normal physiologic conditions reported in Table 4.3 (determined for model input $[\mathrm{Phe}]_{\mathrm{ss}}^{\mathrm{P}}$= 77 μM, $[\mathrm{CL}]_{\mathrm{ss}}^{\mathrm{P}}$= 739 μM and c_f=0 [84, 92]).

To further investigate the effect of fluctuations, we considered a PKU case for which we fixed the non-fluctuating plasma Phe and CL concentrations and varied the fluctuation indices (fundamental frequency and amplitude-to-mean ratio) of a purely sinusoidal signal oscillation, $[\mathrm{Phe}]_{\delta}^{\mathrm{P}} = \sin(2\pi f_0 t)$, within realistic bounds ($0.14 \leq f_0 \leq 7$ cycles per day and $0 \leq c_f \leq 1$) [129, 144-147]. We similarly calculated the fluctuating and steady state concentrations of Phe and CL in the NVU compartments. For each compartment, we calculated the root mean square of the difference between the fluctuating and steady state responses (normalized with respect to normal physiologic conditions) and considered it as a metric for the excursion of the concentration of Phe and CL.

Finally, we employed the model to investigate the impact of therapeutic supplementation of non-Phe LNAAs on the concentrations of Phe and CL in NVU cells. To this end, we considered the supplemented LNAAs (SL) as CL with the same kinetics, and prescribed it as constant input (representing the effective plasma concentration of SL) to the model. We then determined steady state and fluctuating responses in the NVU, considering, as model input, different values for the effective steady state concentrations of SL in the plasma (0.5, 2 and 5 mM) and of both steady state ($[\mathrm{Phe}]_{\mathrm{ss}}^{\mathrm{P}}$ =1000 and c_f= 0) and sinusoidally fluctuating plasma Phe concentration

($[\mathrm{Phe}]_{\delta}^{\mathrm{P}} = \sin(2\pi f_0 t), [\mathrm{Phe}]_{\mathrm{ss}}^{\mathrm{P}}$ =1000 μM, c_f= 0.5 and f_0= 1 cycles/day). We show the responses as time series (excluding transition from steady state) normalized with respect to the corresponding values of baseline physiologic conditions.

Sensitivity analysis:

We evaluated the sensitivity of the reported results on the choice of literature-reported model parameter values. To this end, we calculated model output for 100 cases in which the nominal model input parameters (maximum transport rates, Michaelis-Menten binding constants and steady state physiologic concentration values of LNAAs in individual compartments (Tables 1 and 3) were varied randomly in a range of ±20% from their respective nominal values. In the results, the shown upper and lower bounding curves correspond to standard deviations of the calculated concentrations from those computed under nominal parameter conditions.

Table 4.1. Model parameters

	Value	Unit	Reference
LAT1 (MBEC)			
$K_{m,abs,LAT1,Phe}^{P(ISF)}$	11	μM	[25]
$V_{max,LAT1,lum,Phe}$	0.075	μmol/min	[25, 104]
$K_{m,abs,LAT1,CL}^{P(ISF)}$	52.9*	μM	[25]
$V_{max,LAT1,lum,CL}$	0.129*	μmol/min	[25, 104]
RK_{LAT1}	80	-	[137]
LAT2 (Astrocyte)			
$K_{m,abs,LAT2,Phe}^{ISF(Ast)}$	110.2*	μM	[28]
$V_{max,LAT2,Phe}$	0.1128	μmol/min	[59, 105]
$K_{m,abs,LAT2,CL}^{ISF(Ast)}$	185.9*	μM	[28]
$V_{max,LAT2,CL}$	0.1494*	μmol/min	[59, 105]
B^0AT2 (Neuron)			
$K_{m,abs,B^0AT2,Phe}^{ISF(Neu)}$	1050	μM	[32]
$V_{max,B^0AT2,Phe}$	0.0086*	μmol/min	[32, 106]
$K_{m,abs,B^0AT2,CL}^{ISF(Neu)}$	126.2*	μM	[32]
$V_{max,B^0AT2,CL}$	0.0186*	μmol/min	[32, 106]
$K_{m,B^0AT2,Na}^{ISF(Neu)}$	1050	μM	[107]
$\Delta\Psi$	-70	mV	[108]
β	0.6*	mV	[94, 107]
$[Na]^{ISF}$	141	mM	[109]
$[Na]^{Neu}$	40	mM	[110]
V_{MBEC}	3.5	μl	[109, 111]
V_{ISF}	352.6	μl	[104, 112]
V_{Ast}	742	μl	[113, 114]
V_{Neu}	441.7	μl	[114-116]

*The details of calculation processes are reported in [137] .

Results

NVU steady state condition in relation to steady state plasma Phe concentration

Figure 4. 2 shows plots of steady state concentrations of Phe and CL in neurons versus steady state concentrations of plasma Phe in the range between 77 μM (normal physiologic conditions) to values above 1200 μM (severe classic PKU). Concentrations in the other compartments are shown in Figure 4.S1 in the online Supplementary information. In all NVU compartments, Phe concentration increases with its plasma concentration, while the opposite behavior is observed for CL. In Fig. 4.S1E, we show the steady state responses in the whole brain tissue as volume-weighted average of the steady state responses in the individual NVU compartments. Given that animal species are different in terms of NVU geometry and also kinetic characteristics of LNAA transporters [25, 148, 149], a 1:1 comparison between various species cannot be provided for concentration behavior of LNAA in the brain. However, the observed

growth trend we determined for Phe in whole brain tissue in our in silico adult PKU rat brain model is qualitatively in line with experimental observations in a PKU mouse model [140].

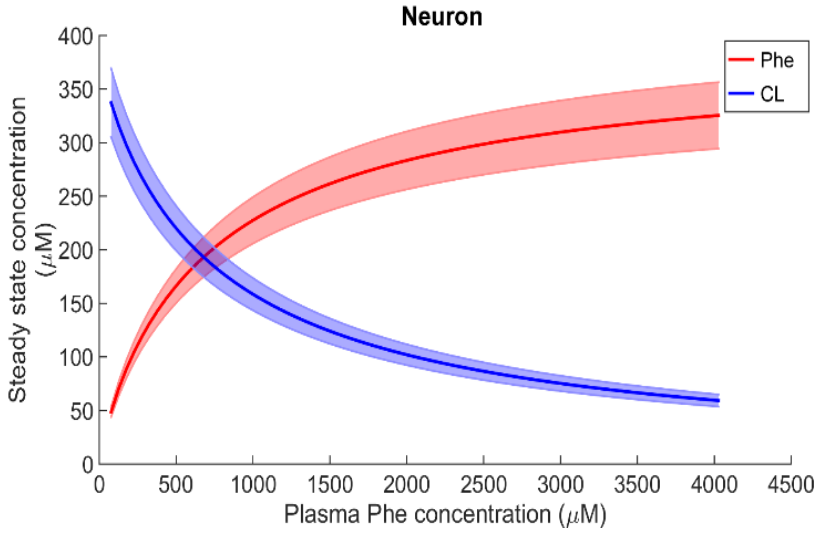

Figure 4.2. Model calculation of the steady state concentration of Phe and CL in neurons in relation to Phe concentration in the plasma. The bold solid lines correspond to results obtained with nominal model parameter values. The lower and upper bounds indicate standard deviation determined by sensitivity analysis (see Methods). Similar relations between Phe and CL steady state concentrations are also observed in the other NVU compartments (see Fig. 4.S1 in the online Supplementary information).

Table 4.2. Fluctuation indices of exemplary Phe plasma concentration profiles

Case number	(μM)$[\mathrm{Phe}]_{\mathrm{ss}}^{\mathrm{P}}$	(cycles/day)f_0	(-)c_f
c1	300	1	0.99
c2	800	3	0.3
c3	1600	0.14	0.6

The dynamics of LNAAs in the NVU are influenced by Phe concentration fluctuations in the plasma.

After the assessment of the NVU steady state response to steady state plasma Phe concentrations, we calculated the dynamic changes of Phe and CL in the NVU in response to plasma Phe fluctuations. Figure 4.3 shows the evolution of the concentrations of Phe and CL over time in MBECs (Fig. 4.3B,1-3), brain ISF (Fig. 4.

3C,1-3), astrocytes (Fig. 4.3D,1-3) and neurons (Fig. 4.3E,1-3) for the three plasma Phe fluctuation cases c1, c2 and c3 (Fig. 4.3A,1-3) (normalized with respect to normal physiologic conditions) over a span of 14 days. The shown upper and lower bounding curves correspond to standard deviations investigated through sensitivity analysis (see Methods). In all cases, the results highlight the competition between Phe and CL: for example, the transfer of Phe through MBEC via the antiporter LAT1 is associated with movements of CL in reverse direction at both luminal and abluminal BBB membranes (Fig. 4.3B1-3). Once Phe and CL gain entry into the brain ISF (Fig. 4.3C1-3), they are either exchanged back into MBECs through abluminal LAT1 (Fig. 4.3B1-3) and/or astrocytes via LAT2 (Fig. 4.3D1-3), and/or co-transported along with sodium ions into neurons via B^0AT2 (Fig. 4.3E1-3). Additionally, in all cases, the steady state Phe concentration in brain ISF, astrocyte and neurons are characterized by values higher than under normal physiologic conditions (which correspond to 'baseline' or 100% in the figure), while the opposite is observed for CL concentrations. We also observe that the concentration dynamics of both Phe and CL in the NVU compartments are influenced by plasma Phe fluctuations, with the impact dependent on plasma Phe fluctuation frequency, mean value, and amplitude-to-mean ratio. For example, in case c1, plasma Phe fluctuations strongly affect the dynamics of Phe and CL concentration in brain ISF and MBECs and, to a lesser extent, in astrocytes and neurons. In case c2, the variations in concentrations of Phe and CL in astrocyte and neurons are not significant as compared to corresponding changes in MBECs and brain ISF. Finally, in case c3, we observe large variations in concentrations of Phe and CL in brain ISF and MBEC, but comparably lower variations in astrocytes and neurons.

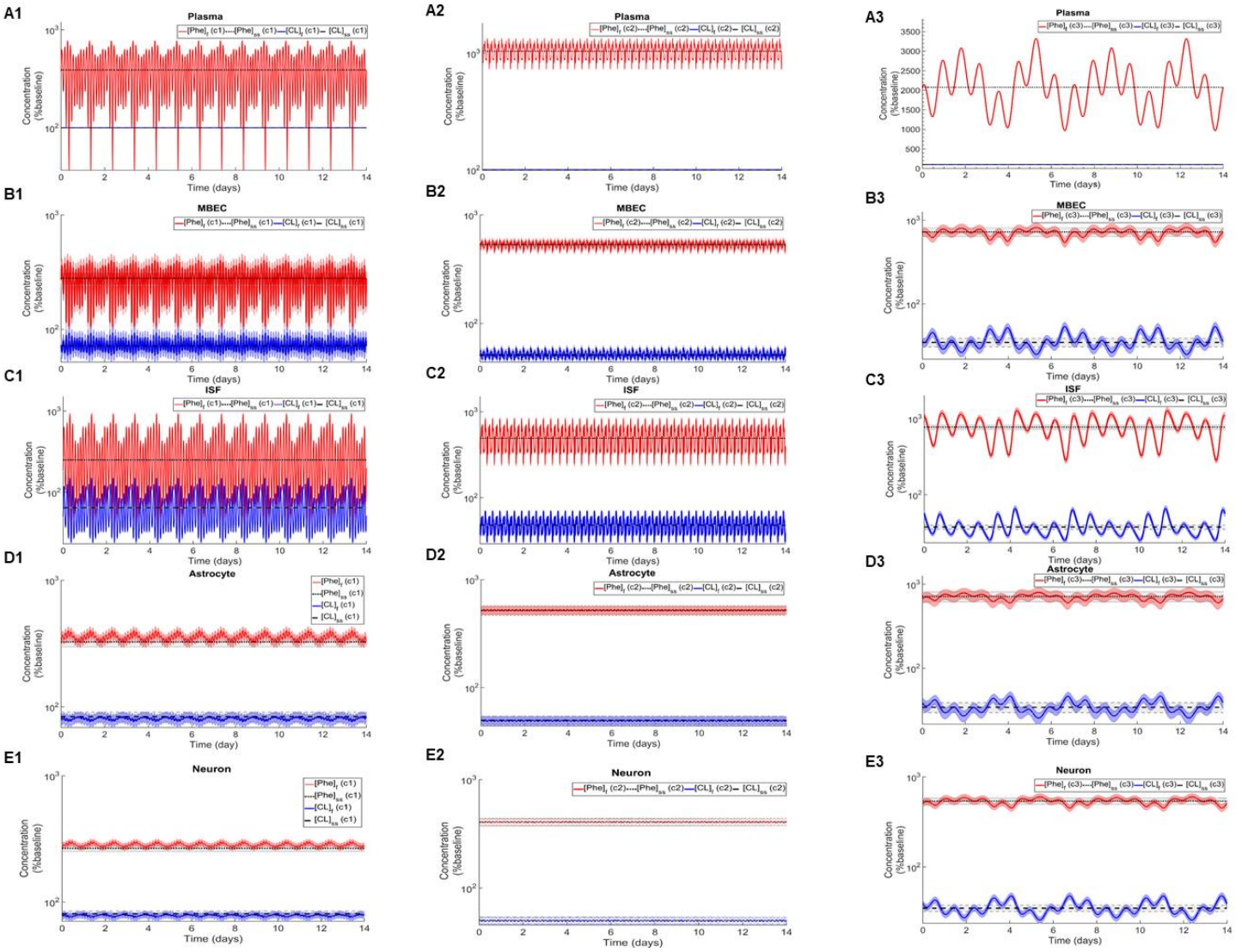

Figure 4.3. Dynamic changes in the concentrations of Phe and CL in MBECs, ISF, astrocytes and neurons in response to fluctuations of Phe concentration in the plasma. Panel (A) shows the plasma concentration of L-phenylalanine (Phe) and competing LNAAs (CL) for the three cases c1, c2, and c3 described in the Methods. For each case, panels B1-3, C1-3, D1-3 and E1-3 show, respectively, the computed steady state concentrations of Phe and CL concentrations ($[\mathrm{Phe}]_{\mathrm{ss}}$ and $[\mathrm{CL}]_{\mathrm{ss}}$) as well as the fluctuating response ($[\mathrm{Phe}]_{\mathrm{f}}$ and $[\mathrm{CL}]_{\mathrm{f}}$) in MBECs, ISF, astrocytes and neurons. The lower and upper bounds indicate standard deviation determined by sensitivity analysis (see Methods). The physiologic baseline concentrations of Phe and CL are reported in Table 4.3.

Association between plasma Phe fluctuation and changes in Phe and CL concentration in the NVU

To study how perturbations in Phe and CL concentrations in the NVU relate to plasma Phe fluctuation indices, we simultaneously varied f_0 and c_f of sinusoidally fluctuating plasma Phe concentration, and then calculated the corresponding changes in concentration of Phe and CL in the NVU compartments. We thereby quantified the associations between Phe and CL excursion and the plasma Phe frequency and amplitude-to-mean ratio. Figure 4.S2 shows corresponding results observed over a span of 14 days ($[\mathrm{Phe}]_{\delta}^{\mathrm{P}} = \sin(2\pi f_0 t)$ and $[\mathrm{Phe}]_{\mathrm{ss}}^{\mathrm{P}}$ =1600 μM). The largest Phe and CL changes are observed in all NVU compartments for large amplitude-to-mean ratio of Phe fluctuations in the plasma. Additionally, low frequencies lead to higher excursion for Phe and CL in astrocytes and neurons and also in ISF for CL, whereas in the same ISF compartment the Phe excursions are lower under low frequencies (Fig. 4.S2, panels, B1-2, C1-2, D1-D2). Finally, we observed that in MBECs, excursion levels are not influenced by the fluctuation frequency and that the changes in Phe and CL concentration are also not significantly sensitive to fluctuation frequency in the other compartments when the fluctuation coefficient is small (Fig. 4. S2, A1-D2).

Table 4.3. Steady state normal physiologic (baseline) concentration values of Phe and CL in the NVU

Compartment	Parameter	Concentration			Unit
Microvascular brain endothelial cell	$[\mathrm{Phe}]_{\mathrm{ss}}^{\mathrm{MBEC}}$	146.8	±	24.6	μM
	$[\mathrm{CL}]_{\mathrm{ss}}^{\mathrm{MBEC}}$	1408.8	±	235.7	μM
Brain interstitial fluid	$[\mathrm{Phe}]_{\mathrm{ss}}^{\mathrm{ISF}}$	0.4	±	0.03	μM
	$[\mathrm{CL}]_{\mathrm{ss}}^{\mathrm{ISF}}$	3.8	±	0.3	μM
Astrocyte	$[\mathrm{Phe}]_{\mathrm{ss}}^{\mathrm{Ast}}$	40.6	±	4.8	μM
	$[\mathrm{CL}]_{\mathrm{ss}}^{\mathrm{Ast}}$	389.7	±	46.0	μM
Neuron	$[\mathrm{Phe}]_{\mathrm{ss}}^{\mathrm{Neu}}$	53.4	±	7.0	μM
	$[\mathrm{CL}]_{\mathrm{ss}}^{\mathrm{Neu}}$	368.7	±	46.9	μM

The details for the calculation of the steady state conditions are reported in [137]. The plasma concentrations of Phe and CL are 77 and 739 μM, respectively [84, 92].

Impact of LNAA supplementation on Phe and CL concentrations in the NVU

To elucidate the impact of non-Phe LNAA supplementation, we determined Phe and CL concentrations in neurons (Fig. 4.4B1,2), MBECs (Fig. 4.S3B1,2), ISF (Fig. 4. S3C1,2) and astrocytes (Fig. 4. S3D1,2) in response to various concentrations of SL in the plasma under both steady state and fluctuating Phe conditions (Fig. 4.4A1,2).

The shown upper and lower bounding curves correspond to standard deviations investigated by performing sensitivity analysis. Our results show that supplementation of LNAA attenuates the disturbed steady state concentration of Phe and CL in the NVU and modulates their concentrations towards physiologic baseline conditions (Table 4.3). This is due to the reason that SL together with CL increases the competitions between Phe and non Phe LNAAs through LAT1 across the BBB and thereby inhibits LAT1 mediated trans-endothelial transport of Phe fluctuations from plasma into the brain. As a consequence, this leads to a reduction in the amplitude level of Phe and CL fluctuations in neurons, MBECs, ISF and astrocytes (Figs. 4.4B1-2, Fig. 4.S3B1-2, S3C1-2 and S3D1-2, respectively). In addition, the increased competition via LAT1 leads to delayed response in neurons, ISF and astrocytes (Figs. 4.4B1-2, Fig. 4.S3C1-2 and S3D1-2, respectively).

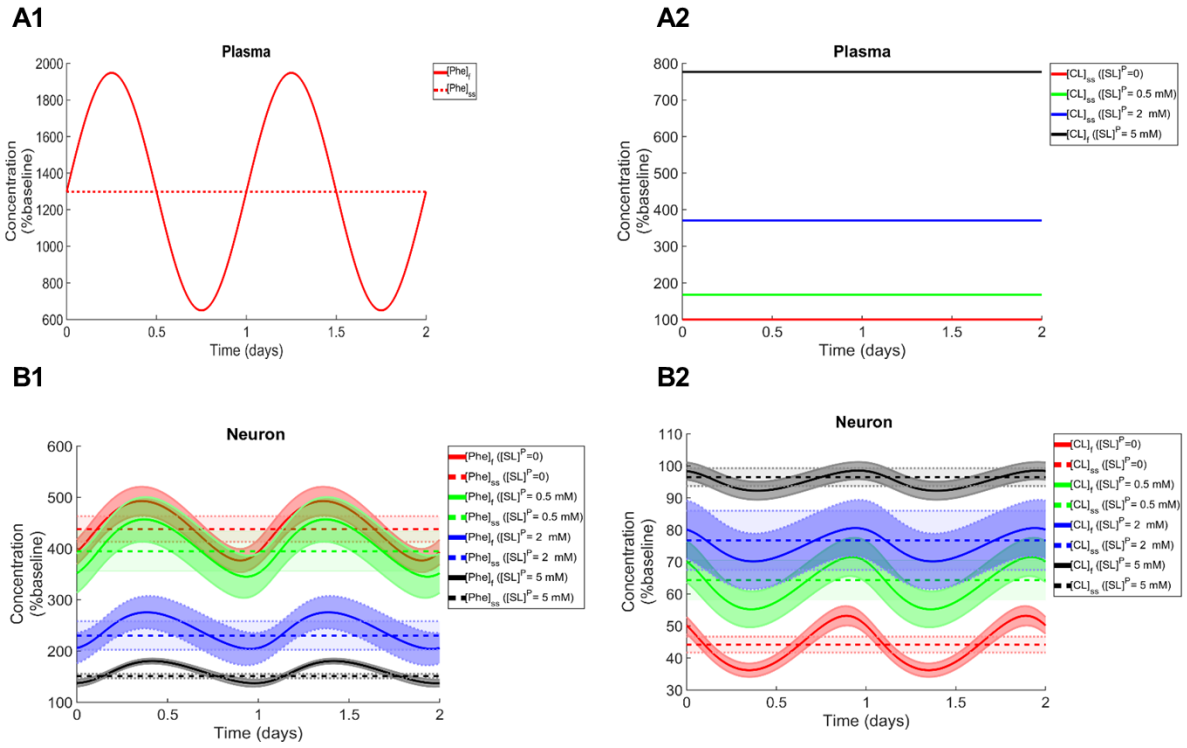

Figure 4. 4. Impact of LNAA supplementation on Phe and CL concentrations in the NVU. Panels (A1, 2) show the plasma concentration of L-phenylalanine (Phe) and competing LNAAs (CL) used as model input. Panels (B1, 2) show the model calculations for steady state concentrations of Phe and CL ($[\mathrm{Phe}]_{\mathrm{ss}}$ and $[\mathrm{CL}]_{\mathrm{ss}}$) as well as the fluctuating response ($[\mathrm{Phe}]_{\mathrm{f}}$ and $[\mathrm{CL}]_{\mathrm{f}}$) in the neuronal compartment for various

concentration levels of supplemented LNAAs in the plasma ($[\mathrm{SL}]^{\mathrm{P}}$). The lower and upper bounds indicate standard deviation determined by sensitivity analysis (see Methods). In all panels, the baseline physiologic concentrations of Phe and CL are reported in Table 4.3.

Discussion

Failure of AA homeostasis in general negatively affects cell function [150]. In cells of the NVU, Phe and CL are involved in a variety of processes, including the synthesis of essential neurotransmitters such as dopamine (3-hydroxytyramine) and serotonin (5-hydroxytryptamine; 5-HT) [151-154], and the production of proteins and lipids (e.g., myelin) [125, 126], although their function in the latter processes is not fully understood. Hence, depending on the full set of roles of Phe and CL, oscillations of their concentrations in the NVU could have a negative impact on central nervous system (CNS) function. However, fluctuating NVU-LNAA concentrations are difficult to measure in animal models of PKU. Furthermore, in patient studies, the effects of elevated steady state plasma Phe concentration cannot be easily differentiated from those caused by increased fluctuations in Phe. The here introduced *in silico* model can serve as an alternative tool to probe these complex dynamics quickly and quantitatively.

We first showed that with increasing Phe concentration in plasma, the steady state concentration of Phe in the NVU and in whole brain increases, while CL concentration decreases. The growth trend we determined for Phe in our *in silico* adult PKU rat brain model is qualitatively in line with experimental observations in a PKU mouse model [140]. We then showed that the propagation of plasma Phe concentration oscillations into the NVU largely depend on fluctuation indices such as frequency and amplitude-to-mean ratio. We observed the largest Phe and CL concentration excursions in the NVU for low frequencies and large amplitude-to-mean ratios of plasma Phe fluctuations. Additionally, we observed that, for the small fluctuation coefficients, the sensitivity of Phe and CL excursions to plasma Phe fluctuation frequency is not significant. Finally, we showed that supplementation of LNAAs not only reduces steady state concentrations in the NVU towards normal physiologic values, but also leads to a reduction in Phe and CL fluctuation amplitude. In conclusion, our *in silico* experiments support LNAA supplementation as therapeutic strategy for reducing the propagation of

plasma Phe concentration fluctuations into the brain. The model itself can also be seen as a potential stepping-stone for the development of a patient-specific LNAA supplementation treatment-planning tool.

The computational model has been built on a number of simplifying assumptions. In particular, we focused on the pathways mediated by dominant transporters and thus disregarded pathways related to metabolism, diffusion and NVU transporters with low levels of expression, which have been shown to be of lesser importance [96, 127]. Additionally, we considered Phe and CL as a homogenous mixture within the individual NVU components. Furthermore, we considered CL as a single entity rather than accounting one by one for each individual competitor, i.e. for L-isoleucine, L-tyrosine and others. The validity of these assumptions are discussed in more detail in [137]. To account for effects of uncertainties associated with the values of the model parameters, we have performed a sensitivity analysis demonstrating that our conclusions are robust with respect to reasonable parameter variations.

Summary

Using a computational model of adult rat NVU-LNAA homeostasis, we investigated the effects of plasma Phe fluctuations on the dynamics of LNAAs in MBECs, brain ISF, astrocytes and neurons in phenylketonuria. Comparable *in vivo* investigations are not readily doable with current techniques. Our results show that plasma Phe fluctuations can propagate into the NVU and change there the concentration of LNAAs, with the magnitude of this effect largely dependent on the frequency and amplitude-to-mean ratio of the plasma concentration fluctuations. Finally, we quantified the therapeutic impact of supplementation of LNAAs in attenuating the disturbed fluctuating and steady state concentrations of Phe and CL in the cells of NVU in PKU disorder towards normal physiologic levels.

Acknowledgments

We kindly acknowledge the financial support from SystemsX.ch - The Swiss Initiative in Systems Biology through the QuantX project, and from the Swiss National Science Foundation through NCCR Kidney.CH and grant 310030_166430.

Author Contributions

M.T. implemented the computational model and performed the calculations with S.B.. F.V. and V.K. directed the research, contributing equally. All authors conceived and designed the study, analyzed the data, wrote the manuscript and approved the final version.

Conflict of interest

The authors declare that they have no conflict of interest.

Supplementary information

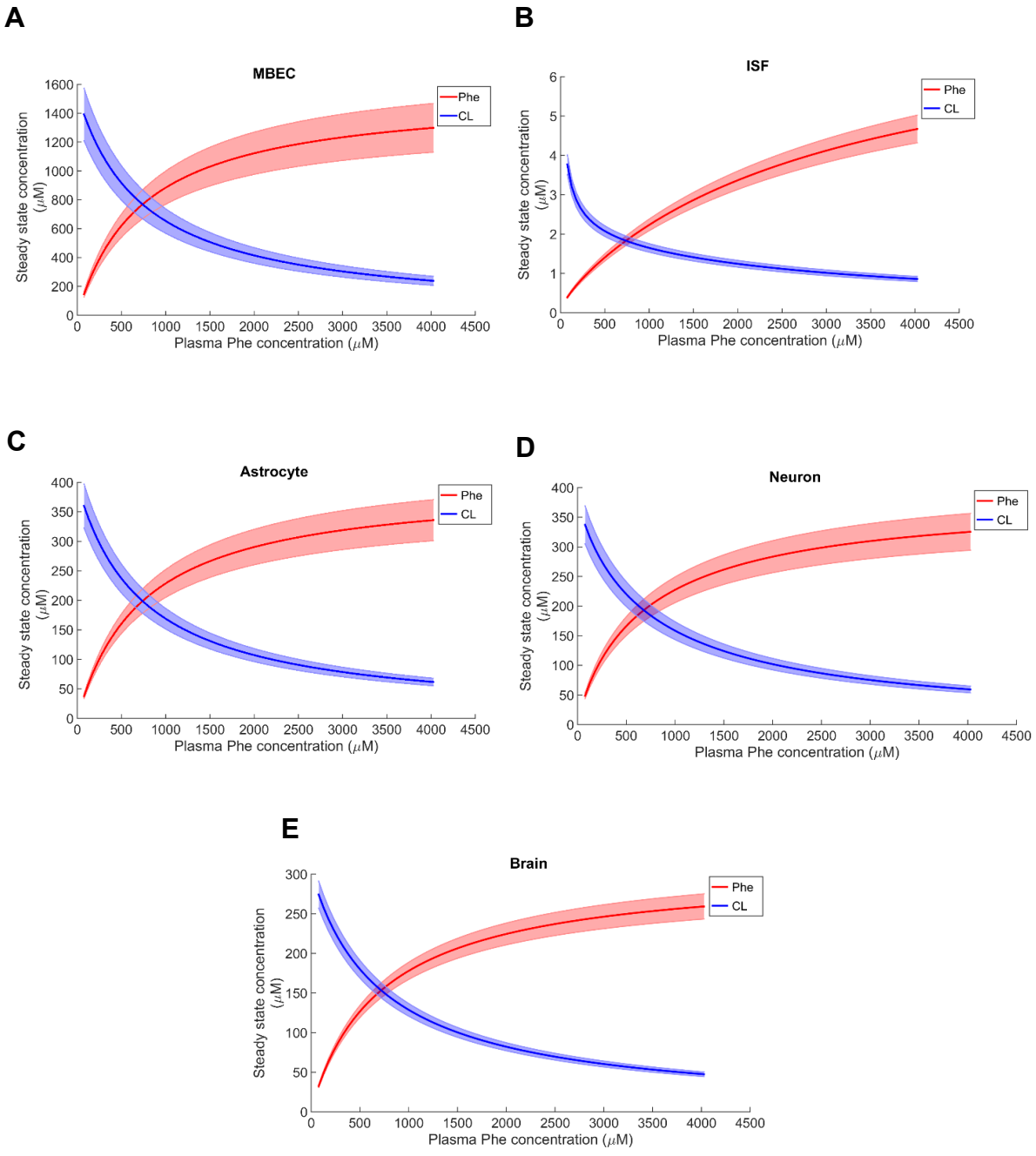

Figure 4. S1. Steady state concentration of Phe and CL in MBECs, ISF, astrocytes and neurons and whole brain in relation to Phe concentration in the plasma. Panels A to E show model calculations for the steady state concentrations of Phe and CL in MBECs (panel A), ISF (panel B), astrocytes (panel C), neurons (panel D) and the whole brain (panel E). The bold solid lines correspond to results obtained with nominal model parameter values. The lower and upper bounds indicate standard deviation determined by sensitivity analysis (see Methods).

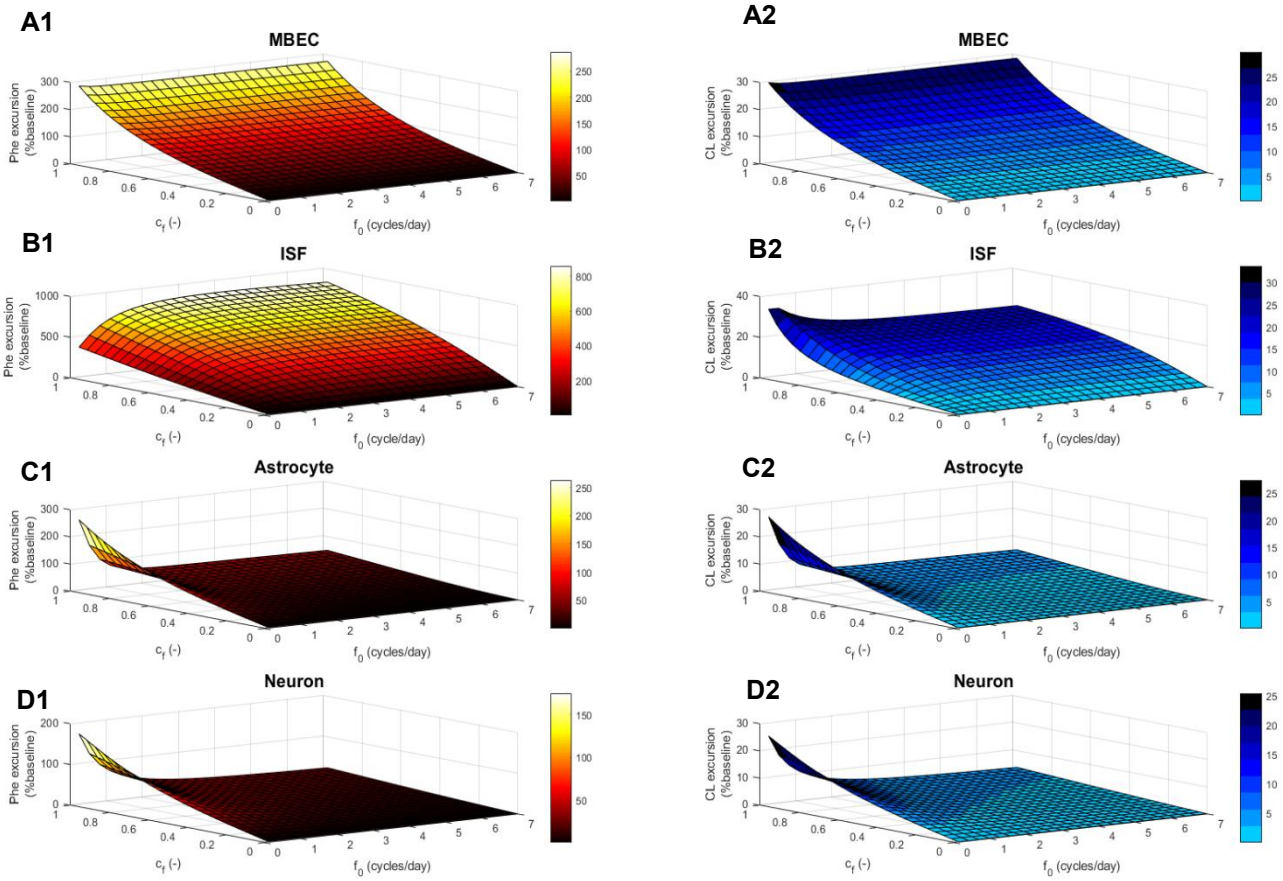

Figure 4. S2. Phe and CL excursion in the NVU compartments in relation to the plasma Phe fluctuation indices. Panels A to D show model calculations for Phe (left column) and CL excursion (right column) in the NVU compartments as a function of fundamental frequency (f_0) and amplitude-to-mean ratio (c_f) of Phe in the plasma (see Methods for definition of 'excursion'). The results are normalized with respect to normal physiologic concentrations (baseline).

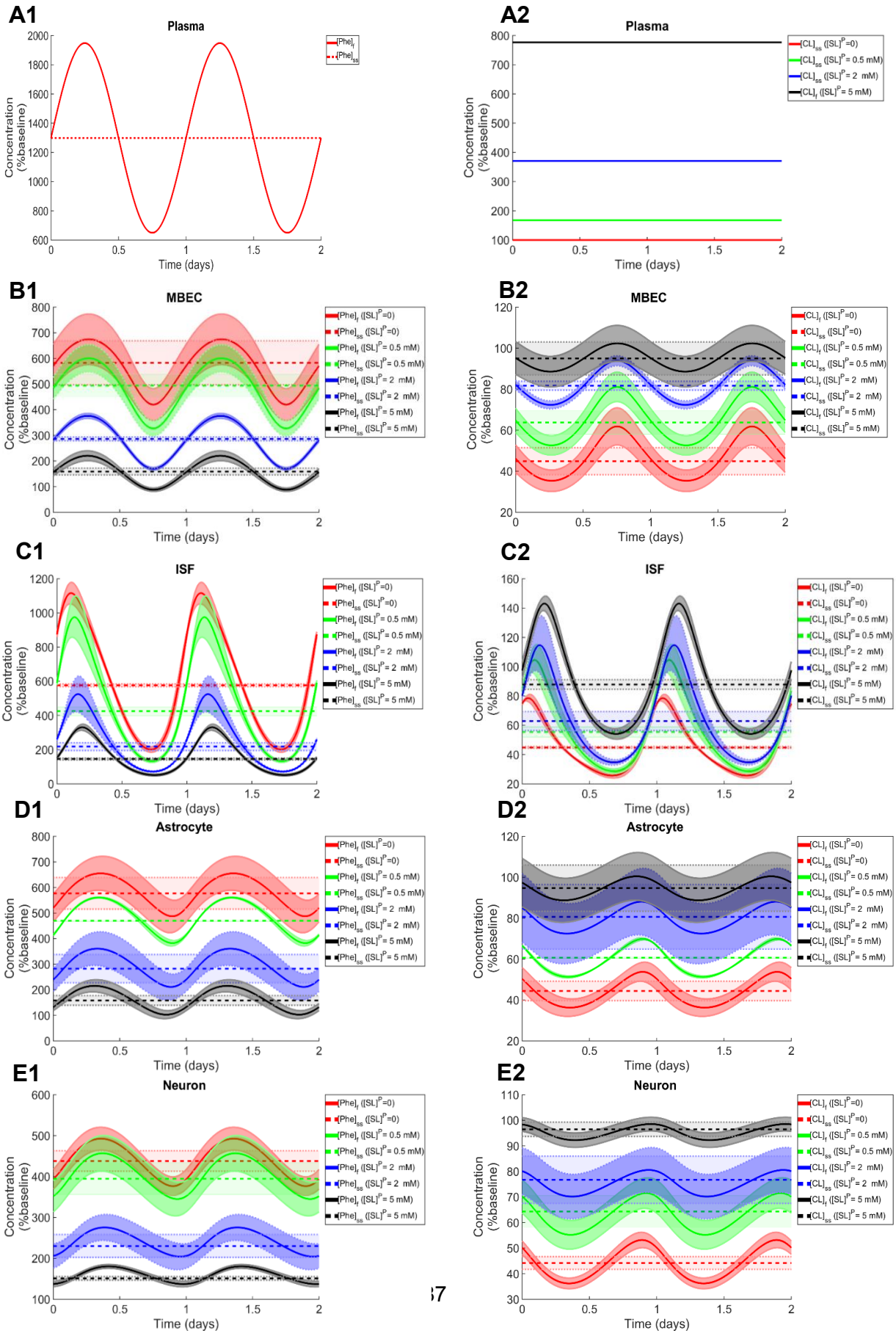
A1
Plasma
Concentration (%baseline)
Time (days)
A2
Plasma
Concentration (%baseline)
Time (days)
B1
MBEC
Concentration (%baseline)
Time (days)
B2
MBEC
Concentration (%baseline)
Time (days)
C1
ISF
Concentration (%baseline)
Time (days)
C2
ISF
Concentration (%baseline)
Time (days)
D1
Astrocyte
Concentration (%baseline)
Time (days)
D2
Astrocyte
Concentration (%baseline)
Time (days)
E1
Neuron
Concentration (%baseline)
Time (days)
E2
Neuron
Concentration (%baseline)
Time (days)

Figure 4. S3. Impact of LNAA supplementation on Phe and CL concentrations in the NVU. Panels (A1, 2) show the plasma concentration of L-phenylalanine (Phe) and competing LNAAs (CL) used as model input. Panels (B1, 2), (C1, 2), (D1, 2) and (E1, 2) show the model calculations for steady state concentrations of Phe and CL ($[\mathrm{Phe}]_{\mathrm{ss}}$ and $[\mathrm{CL}]_{\mathrm{ss}}$) as well as the fluctuating response ($[\mathrm{Phe}]_{\mathrm{f}}$ and $[\mathrm{CL}]_{\mathrm{f}}$) in the NVU compartments for various concentration levels of supplemented LNAAs in the plasma ($[\mathrm{SL}]^{\mathrm{P}}$). The lower and upper bounds indicate standard deviation determined by sensitivity analysis (see Methods). In all panels, the baseline physiologic concentrations of Phe and CL are reported in Table 3.

Chapter 5 Conclusion and outlook

Conclusion

The focus of this doctoral thesis is to establish a combined computational and experimental framework of AAT interactions to investigate the regulation of amino acids (AAs) across cell membranes. The first part of the thesis (chapter 2) introduced an integrated *in vitro* and *in silico* approach that enables unraveling the contributions of specific players in a complex cellular network of AAs and AATs at single membranes. The second part (chapter 3) described a combined *in vivo* and *in silico* approach to investigate the dynamic interactions between large neutral amino acid (LNAA) transporters located at the membranes of neurovascular unit (NVU) cells. The third part (chapter 4), presented an application for the *in silico* model of large neutral amino acid (LNAA) homeostasis in the NVU to gain some insights into the regulatory role of brain LNAA transporters involved in Phenylketonuria (PKU) disorder.

In chapter 2, we provided a robust and versatile tool based on a systems biology approach to characterize the contributions of specific AAT to overall cellular transport, using limited experimental input. Using this approach, we could accurately predict the cellular transport responses to new stimuli in presence and absence of extracellular sodium ions and different competitive inhibitors. We applied this strategy to quantify L-leucine and L-phenylalanine individual AATs expressed in *X. leavis* oocyte *in vitro*. However, given the appropriate assay conditions, this methodology is also applicable to other enzymes, substrates, and/or cellular systems where the kinetics of each active enzyme species in the system can be described by the Michaelis–Menten equation. While the main strength of our approach is its capability to quantify the activity of individual transporters that function within a complex network of transporters, it is limited to the investigation of the trans-membrane transport processes through single membranes and under steady state conditions where the MM assumptions are valid.

In chapter 3, we further extended our mathematical model beyond the Michaelis–Menten kinetics to represent dynamics of AATs interactions through multiple cell membranes. We have targeted the NVU-LNAA transport system to get more insight on mechanisms that maintain the homeostasis of LNAAs in the NVU individual cells, such as microvascular brain endothelial cells (MBECs), astrocytes and neurons. By

incorporation of published *in vivo* microdialysis measurements obtained in rat brain into our newly developed *in silico* model, we have shown that either strong asymmetrical bi-directional kinetics of LAT1 in MBECs (lower affinity inside the MBECs) and/or an asymmetric distribution of LAT1 at both membranes of MBECs (lower expression at the abluminal membrane of the BBB) is required to reproduce published *in vivo* measurements. Our conclusion is supported by data obtained for two different LNAAs, L-tyrosine and L-phenylalanine. This vital characteristic of LAT1 function in MBECs could not be addressed satisfactorily up to now by available *in vivo* and *in vitro* standard assays. LAT1 plays a crucial role in regulating the import and export of a large number of substrates including some prodrugs such as L-DOPA in and out of the brain. Therefore, our observations for its asymmetric kinetics and/or expression could shed lights on LAT1 mediated prodrug delivery across the BBB [120-122]. On the basis of our findings about the function of LAT1 across the BBB, we furthure investigated the dynamics of LNAAs concentrations in MBECs, brain ISF, astrocytes and neurons in response to IP-administered L-tyrosine and L-phenylalanine, values which are difficult and challenging to determine experimentally. Finally, we used our model to explain the trans-stimulation of LNAA uptake across the blood brain barrier (BBB) upon interstitial application of BCH (2-aminobicyclo-(2,2,1)-heptane-2-carboxylic acid), a LAT1 competitive inhibitor. Taken together, our developed *in silico* model of NVU-LNAA homeostasis is shown to circumvent some limitations associated with the available *in vivo* and *in vitro* experimental approaches. Our computational model, however, is not limited to study the cases we reported and it could be further served to mimic more experimental situations. For instance, it can be used to capture the impact of inhibition of LAT1 at the luminal and abluminal membranes of the BBB and/or LAT2 in astrocytes and/or B^0AT2 in neurons, through supplementation of different physiological and non-physiological substrates and thereby to provide a quantitative representation for the corresponding dynamic changes in concentrations of LNAAs in cells of NVU.

In chapter 4, using our NVU-LNAA homeostasis model, we further extended our study to unravel the regulatory role of individual LNAA-NVU transporters in the propagation of abnormal perturbations of Phe from plasma into the NVU individual cells in Phenylketonuria (PKU) disease. We suggested that plasma Phe fluctuations can potentially propagate into the NVU and change there the concentration of LNAAs, with the highest magnitude of this effect at low frequency and high amplitude-to-mean ratio

of the plasma Phe concentration fluctuations. Failure of AA homeostasis in general harmfully affects cell function [150]. In the NVU individual cells, Phe and CL are involved in a variety of processes, including the synthesis of essential neurotransmitters such as serotonin (5-hydroxytryptamine; 5-HT) and dopamine (3-hydroxytyramine) [151-154], and the production of proteins and lipids (i.e., myelin) [125, 126], although their function in the latter processes is not completely characterized. Therefore, depending on the full set of function of Phe and CL, fluctuations of their concentrations in the NVU could have a negative impact on the brain function. Finally, we explained the therapeutic impact of LNAAs supplementation in attenuating the disturbed concentrations of Phe and CL in the MBECs, ISF, astrocytes and neurons in PKU disorder towards normal physiologic levels, something out of reach of *in vivo* techniques. It has to be pointed out while our *in silico* model has been employed in PKU disease, it could potentially be applied to provide new insights into the pathophysiology of other metabolic disorders affecting the brain, such as Maple syrup urine disease (MSUD), that are sensitive to the plasma levels of LNAAs [123].

In conclusion, given the inherent functional complexities associated with the behaviour of AAT systems, there are technological hurdles that need to be overcome to enable corresponding experiments. As an alternative approach, this thesis demonstrates the capabilities of integration of *in silico* with *in vitro* and *in vivo* methods to go around these hurdles and thereby to provide novel insight into the physiological aspects of AAT systems.

Outlook

The computational models we have developed in this thesis as any other model have their simplifications and limitations that are clearly mentioned in each chapter. In particular, the computational models rely on literature-reported parameter values, which are inevitably associated with the reported uncertainty. We handled this limitation through performing sensitivity analysis for each model and demonstrated that the conclusions drawn in this thesis hold within the reported reasonable parameter variations. Also, as it is a common characteristic of biological models, we have built our *in silico* frameworks based on a simplified anatomy of understudied transport

systems. For instance, we have modeled the NVU systems as four compartments (i.e. MBECs, brain ISF, astrocyte and neuron) in which the distribution of LNAAs is considered to be homogenous. In reality, however, regional distribution of AAs may affect their binding efficiency to the corresponding AATs, and therefore also the local transport fluxes. On the other hand, there is hope that upon the progress in imaging and biochemistry techniques more information about the local distribution of AAs as well as the cell morphology will be provided in the near future. This evolution might enhance our knowledge about different AAT systems and would allow for more detailed investigation of these systems in more precise biological morphologies. Furthermore, we focused on a single dominant LNAA transporter per membrane of NVU cells (i.e. LAT1 for MBECs, LAT2 for astrocytes and B^0AT2 for neurons), and thus disregarded the pathways related to diffusion and also NVU transporters with low levels of expression, whose impacts have been shown, however, to be insignificant for LNAAs in the NVU [96, 127]. Moreover, it has to be pointed out that our computational models are developed based on the available literature about the identified AATs and the structure and kinetics of many SLC transporters, including AATs, have yet to be fully characterized, such that further research is required. The contribution of newly discovered AATs, upon appropriate investigation of their kinetic functions, could then be included in our developed computational models.

It has to be emphasized that the approaches developed in this thesis are not limited to the study AAT systems, but they theoretically could be applied to a variety of SLC transport systems functioning in different cell types. For example, our systems biology approach described in chapter 2) could be employed to quantify the relative contribution of a specific SLC peptide (or drug) transporter within a complex network of peptides (or drugs) and SLC transporters functioning at single membranes. Our integrated *in silico* and *in vivo* approach described in chapter 3, for example, could potentially be applied to get more insights into the regulatory roles of SLC glucose (or drug) transporters in the maintenance of glucose (or drug) homeostasis in the NVU. Moreover, our computational approaches can potentially be used to study SLC transport processes across various biological systems such as kidney, intestine, etc. Similar to the situation we faced with NVU-LNAA transport systems, this would significantly depend on the availability of sufficient in vivo experimental data including

results of dynamic time course measurements of concentration changes of the considered substrates, such as AAs, peptide, etc as well as on accurate information about the kinetics of the expressed SLC transporters. Taken together, our studies provide several examples of integrating computational and experimental approaches for studying SLC transport complex systems and demonstrate how this integration could be an excellent asset for basic and applied research.